

A Compact Flicker-Free Transformer-Less LED Driver With an Enhanced Power Factor for Omnidirectional Multichannel Smart Bulb Applications

Younghun Ko, Hong-Soo Cho, Sang-Sung Lee, So-Bong Shin, Yongchul Song, *Member, IEEE*, and Sang-Gug Lee, *Member, IEEE*

Abstract—In this paper, a flicker-free transformer-less multi-channel light-emitting diode (LED) driver that adopts a new power factor enhancement technique is presented. The proposed LED driver divides the transmission path of the current to the LED string in two ways depending on the instantaneous input voltage in order to improve the PF relative to that of a conventional compact flicker-free LED driver that uses a fixed LED current regulation scheme with only one electrolytic capacitor. The proposed driver can be implemented with a minimum number of external components leading to a compact module that allows a light bulb with omnidirectional light emission. In order to enhance the expandability of the smart bulb, a conventional buck converter with 3-V output is integrated with the proposed LED driver to supply the peripherals of the module. The proposed LED driver IC is implemented in a $0.35\text{-}\mu\text{m}$ ultrahigh voltage CMOS process and occupies an area of $2.9\text{ mm} \times 2.0\text{ mm}$. A 10-W smart bulb prototype that adopts the proposed LED driver is flicker free and shows a power factor of 0.715 and power conversion efficiency of 77.5% for an ac supply of 120 V.

Index Terms—Flicker, internet of things (IoT), light-emitting diode (LED) driver, power factor (PF), smart bulb, transformer.

I. INTRODUCTION

LIGHT-EMITTING diode (LED) smart bulbs have come into the spotlight due to their key role as a representative example of the upcoming internet of things (IoT) era [1]. The most fundamental function of a smart bulb is dimming (light control) via wireless communication using Bluetooth, Wi-Fi, ZigBee, etc. A more advanced function is providing an access point (AP) to offer wireless connectivity to smart objects through visible light communication [2]–[4]. The smart bulb is a promising AP candidate since it can be installed in any place that requires light, unlike other embedded computing devices for IoT. For traditional LED manufacturers, these demands could be an

Manuscript received June 18, 2015; revised September 3, 2015 and October 6, 2015; accepted November 2, 2015. Date of publication November 5, 2015; date of current version March 2, 2016. Recommended for publication by Associate Editor J. M. Alonso.

Y. Ko and S.-G. Lee are with the School of Electrical Engineering, Korea Advanced Institute of Science and Technology, Daejeon 305-701, Korea (e-mail: gnsstar@kaist.ac.kr; sglee.kaist@gmail.com).

H.-S. Cho, S.-S. Lee, S.-B. Shin, and Y. Song are with Merlot Laboratories Inc., Seoul 153-791, Korea (e-mail: hongsoo.cho@merlotlab.com; sangsung.lee@merlotlab.com; sobong.shin@merlotlab.com; yongchul.song@merlotlab.com).

Color versions of one or more of the figures in this paper are available online at <http://ieeexplore.ieee.org>.

Digital Object Identifier 10.1109/TPEL.2015.2498193

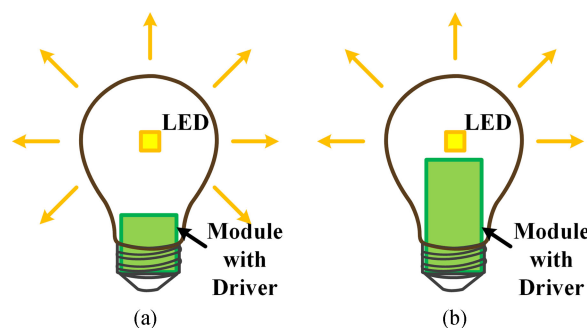


Fig. 1. Examples of LED bulb with (a) compact driver module with omnidirectional light emission and (b) bulky driver module with directional light emission.

opportunity to enter a new market if they can meet the technical demands of smart bulbs. The quality of LED lighting systems can be determined by the commonly used specifications, which are mainly dependent upon LED driver topologies.

Recently, ENERGY STAR has announced specifications for LED light bulbs, which include specific criteria for LED light bulbs that qualify their requirements [5]. The main specifications described in [5] are summarized in the following.

A. Module Form Factor

In [5], the lamps are categorized into omnidirectional, decorative, and directional types depending on the shape of the bulb. For replacing incandescent light bulbs, omnidirectional LED bulbs that provide omnidirectional light emission are preferred. However, the shape of LED bulbs is limited by the size of the driver module, as shown in Fig. 1. Therefore, a LED driver topology that allows a compact module is an essential requirement for omnidirectional indoor LED bulbs. With smart bulbs, omnidirectional bulbs are even more difficult to implement because of the radio components. Fig. 2 shows examples of bulky radio and LED driver modules used in commercial smart bulbs [6].

B. Flicker

Flicker performance should be considered because of growing related health concerns. Flicker refers to a repeated change over time in the brightness of light due to the pulsating LED current

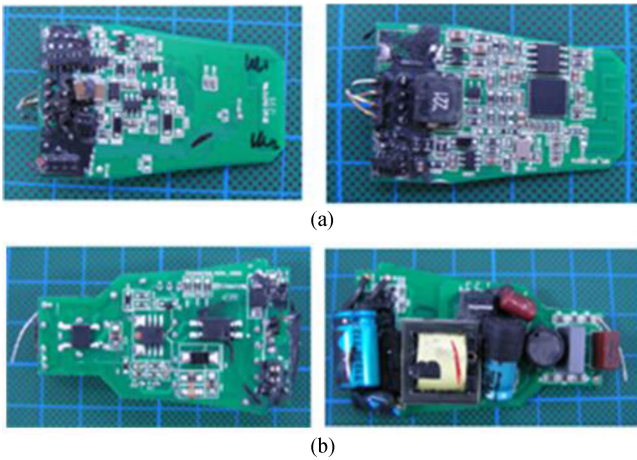


Fig. 2. Examples of (a) radio and (b) LED driver modules used in commercial smart bulbs.

[7]. Percent flicker ($Mod\%$), which is a measure of the cyclic variation in the brightness of light, is defined as $100(A-B)/(A+B)$, where A and B represent the maximum and minimum luminance during one cycle, respectively [5]. Many studies, including [7]–[9], have reported that the low-frequency flicker of less than 200 Hz may induce biological effects such as seizures, epilepsy, headache, eye strain, reduced visual performance, etc., even if it is invisible flicker. In light of these biological concerns, a strict standard for percent flicker was applied in the draft version of [5]. In the final version of [5], however, the flicker requirements have been relaxed to simply report flicker performance to invigorate the LED lighting industry since the standard was considered too difficult to implement with concurrent technology. On the other hand, IEEE standards PAR1789 group presents recommended flicker criteria for flicker frequencies of higher than 90 Hz [8], [9]. For example, the recommended criteria for no-observable-effect level requires the percent flicker that satisfies $Mod\% < 4\%$ where ac line frequency is 60 Hz.

C. Power Factor (PF)

In the ENERGY STAR specifications [5], the PF defined as the ratio of the real power in watts to the apparent power is required to be greater than 0.7. When the input current is a pure sinusoidal and in phase with the sinusoidal input voltage, PF is unity, which can be obtained from a linear load such as pure resistance. The nonlinear loads in a LED lighting system distort the shape of the input current and generate harmonic content, leading to PF degradation. Since a system with a low PF increases generation and transmission costs of power from electric power corporations, a low PF is forced to improve by PF correction (PFC) units which linearize the loads.

D. Luminous Efficacy

The luminous efficacy of a LED lighting system is defined as the ratio of the luminous flux to the real power, which mainly depends on both the LED efficiency and the power conversion efficiency, which in turn depends on the LED driver topology. To satisfy the qualifications of ENERGY STAR, a mini-

um luminous efficacy of 55 lm/W is required for omnidirectional bulbs when the input power is lower than 15 W. In the lighting market, LED bulbs with a luminous efficacy greater than 80 lm/W at an input power of 10 W, which can replace 60-W incandescent bulbs, are preferred. Since the LED efficiency varies depending on the manufacturers, this paper focuses on the power conversion efficiency of LED drivers.

In summary, the module form factor, flicker, PF, and luminous efficacy are used as guidelines in this paper for designing efficient LED drivers, following the specifications of ENERGY STAR.

Depending on the presence of the switched mode power supply (SMPS), LED drivers can be divided into dual-stage ac–dc, single-stage ac–dc, and ac–direct topologies. AC–DC LED drivers normally achieve low flicker by converting sinusoidal ac input into dc supply to regulate the LED current at a constant value. However, usually the PF is very poor, less than 0.65 [10], since a typical ac–dc LED driver consists of nonlinear loads such as transformer, inductor, electrolytic capacitor (e-Cap), etc. Thus, dual-stage ac–dc LED drivers generally adopt the first PFC stage in front of the second dc–dc stage, which provides tightly regulated output current with low current ripple to achieve low flicker. However, the additional PFC stage increases circuit complexity, component count, and cost, and an electromagnetic interference (EMI) filter is necessary since the EMIs caused by the PFC are undesirable, especially for wireless communications. Several dual-stage ac–dc LED drivers [11]–[14] introduce e-Cap-less topologies to expand lifetime of the LED drivers. While the advantages of e-Cap-less topologies have been demonstrated in [11]–[14], the topologies require more complexity leading to the increase in the module size. In summary, considering the number of required external components, the existing dual-stage ac–dc structures are too bulky for the implementation of the omnidirectional indoor LED bulbs. To reduce the module size and cost, single-stage ac–dc LED drivers merge the PFC stage with dc–dc stage. In addition to the advantages of single-stage topologies, several works [15]–[18] have been reported with their own merits, presenting schemes to adopt universal input range using a variable boost inductor [15], improve line regulation [16], cover wide output power range [17], and remove e-Cap [18]. Despite their contributions, flicker-free performance could not be achieved since these works [15]–[18] tend to show higher output current ripple compared to that of dual stage topologies due to the limited value of the output capacitor. On the other hand, ac–direct LED drivers [19]–[22] are suitable for implementing omnidirectional LED bulbs because a high PF can be achieved without requiring bulky PFC units. However, the nature of the LED driving scheme introduces high flicker with low frequency due to the step waveform of the LED current, which harms the human body. In addition to the ac–dc and ac–direct LED drivers, there is another LED driver that allows compact module size and flicker-free performance by adopting only one e-Cap without requiring a transformer. However, this driver is not widely used because of its poor PF, where the waveform of the input current is similar to that of an ac–dc LED driver without PFC. Table I compares the typical characteristics of LED drivers. This work reports the design and

TABLE I
 TYPICAL FEATURES OF LED DRIVERS

	Single-stage ac-dc LED driver	Dual-stage ac-dc LED driver	AC-direct LED driver	e-Cap LED driver
Module form factor	Medium	Bulky	Compact	Compact
Flicker (LED current ripple)	Medium	Low	High	Free
Power factor	> 0.9 with PFC	> 0.9 with PFC	> 0.9	< 0.65

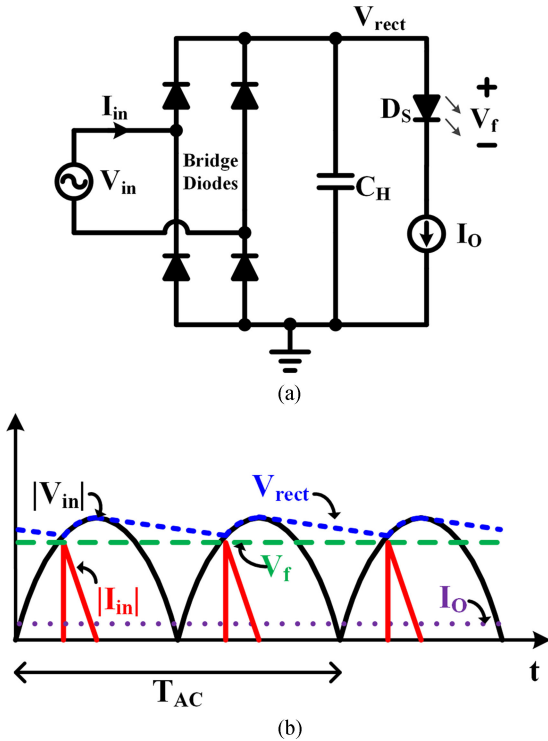


Fig. 3. Conventional e-Cap LED driver (a) circuit schematic and (b) input voltage and current waveforms.

implementation details of an e-Cap-based LED driver with an improved PF while maintaining the inherent compact size and flicker-free characteristics.

This paper is organized as follows. Section II introduces the operational principle of the proposed LED driver. The design details of a smart bulb system that adopts the proposed LED driver are then described in Section III and the experimental results are given in Section IV. Section V concludes the paper.

II. PRINCIPLE OF THE PROPOSED LED DRIVER

Fig. 3(a) shows the circuit schematic of a conventional e-Cap LED driver that consists of bridge diodes, a holding capacitor C_H , an LED string D_S , and a constant current source I_O . When C_H is sufficiently large, the node voltage V_{rect} maintains roughly the peak value of the ac input. If V_{rect} is larger than the LED forward voltage drop V_f , a flicker-free property can be achieved, as shown in Fig. 3(b) because the current flowing through D_S is kept constant during the whole period by I_O . In order for V_{rect} to be larger than V_f for the whole period, the

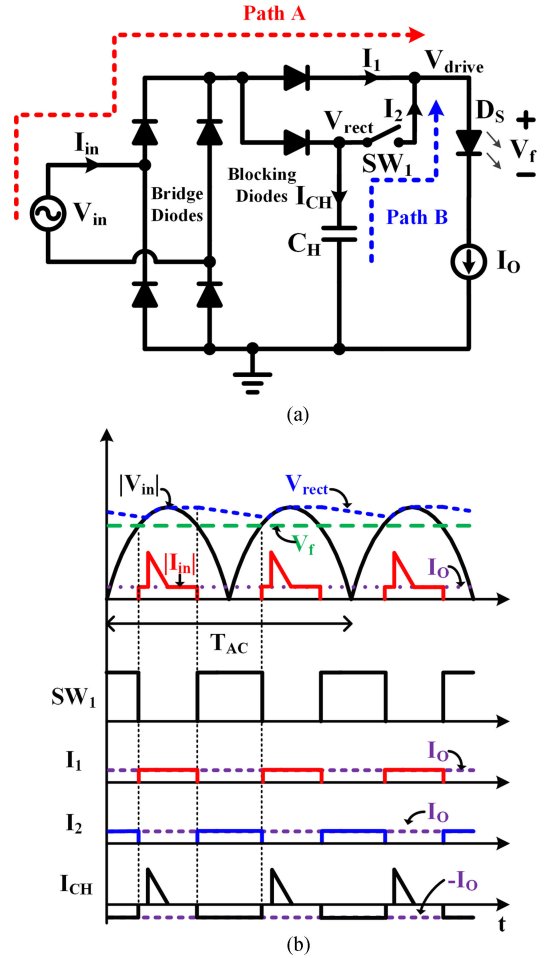


Fig. 4. Proposed flicker-free transformer-less LED driver with PFE. (a) Schematic and (b) key waveforms.

required C_H is given by

$$C_H > \frac{I_O \cdot T_{AC}}{2 \cdot (V_m - V_f)} \quad (1)$$

where V_m is the peak value of the ac input voltage and T_{AC} the period of the ac input. The structure shown in Fig. 3(a) is the simplest LED driver that allows flicker-free performance but small-size implementation using only one e-Cap without requiring a transformer. However, the PF is very poor experimentally, less than 0.65 [10], which is similar to that of an ac-dc LED driver without PFC, since the input current I_{in} that charges C_H is generated over a very short time with a high peak when V_{in} is greater than V_{rect} , and then, I_{in} becomes zero for the rest of the period, while the constant current flowing through the LED is provided from C_H , as shown in Fig. 3(b). Therefore, since this structure cannot achieve a PF greater than 0.7 which is the ENERGY STAR certification standard, a new structure to improve the PF without requiring bulky components for a compact size module is required.

A. Concept of Proposed LED Driver

Fig. 4(a) shows the proposed flicker-free transformer-less LED driver, which consists of bridge diodes, a holding capacitor

C_H , an LED string D_S , a constant current source I_O , two blocking diodes, a switch SW_1 , and a timing generator. First, since the LED current remains constant by the constant current source I_O , the proposed LED driver can achieve flicker-free operation for any positive driving voltage V_{drive} that is larger than V_f . The principle of enhancing PF is increasing the period of the input current generation time and thereby decreasing the peak current, which leads to a reduction of high order harmonics. The proposed scheme can be implemented by dividing the transmission path of the current to D_S in two ways depending on the instantaneous voltage of V_{in} . In Fig. 4(b), when V_{in} is sufficiently large to be able to drive D_S , SW_1 turns OFF and the LED current is supplied through path A directly from the ac input supply. In addition, when V_{in} becomes greater than the voltage across C_H , some I_{in} flows into C_H over a short period of time with a peak current as shown in Fig. 4(b). On the other hand, when V_{in} is insufficient to drive D_S , SW_1 turns ON and the LED current is supplied through path B from C_H . The ON/OFF timing of SW_1 is determined by the timing generator which is described in Section II-C. As shown in Fig. 4(b), the LED current is kept constant as the constant current I_O is supplied alternately through path A and path B. In addition, it can be shown that the period during which the input current is supplied from V_{in} increases significantly with lower peak current compared to that of the conventional structure shown in Fig. 3(b). The proposed LED driver increases the period during which I_{in} is directly supplied into the LED from V_{in} when V_{in} is sufficiently large to drive D_S , in addition to the period of charging C_H from V_{in} . In the conventional structure, on the other hand, I_{in} is generated in a very short time, only when C_H needs to charge, and then I_{in} becomes zero after the peak point of V_{in} , while the LED current is continuously supplied from C_H . As a result, since the waveforms of I_{in} become more similar to that of V_{in} , PF can be significantly improved. Furthermore, a compact size module can be easily implemented compared to the case of SMPS LED drivers. The additionally required components of the proposed driver are an external P-MOSFET as a switch and two external blocking diodes in addition to the basically required components of the conventional structure, as shown in Fig. 3(a).

B. PF Analysis

To quantitatively analyze how the variables affect the driver performance measures such as the PF in the proposed LED driver, the waveforms shown in Fig. 5 are considered; this is a special case where the voltage ripple $V_r = V_m - V_f$. Since the waveform of I_{in} in the proposed LED driver is nonsinusoidal and includes harmonic content, estimating the exact PF value is quite complicated. Thus, the following assumptions are made to simplify the analysis:

- 1) the bridge and blocking diodes operate as a short circuit for any forward bias;
- 2) the forward voltage drop of D_S is fixed at V_f conducting current for voltage larger than V_f ;
- 3) the on resistance of SW_1 is zero and the current source I_O is ideal;

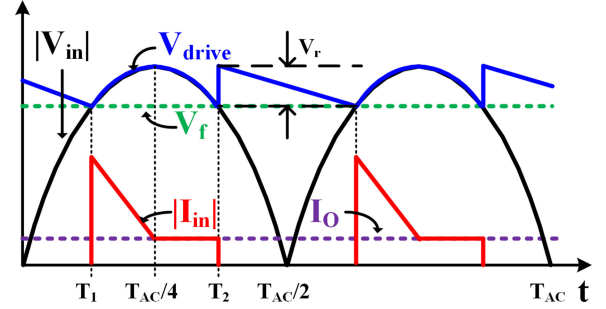


Fig. 5. Key waveforms for PF analysis.

- 4) the analysis is done under a steady-state condition. Thus, the PF is derived from a half period of V_{in} , where $V_{in} = V_m \sin(2\pi t/T_{AC})$;
- 5) for simplicity, the special case where C_H is designed for V_r to be equal to the difference between V_m and V_f , as shown in Fig. 5, is analyzed, where the average of V_{drive} is approximated as $\overline{V_{drive}} = (V_m + V_f)/2$.

Based on above assumptions, the average input power can be given by

$$\begin{aligned} P_{in} &= \frac{2}{T_{AC}} \int_0^{T_{AC}/2} V_{in}(t) \cdot I_{in}(t) \cdot dt = \overline{V_{drive}} \cdot I_O \\ &= \frac{1}{2} (V_m + V_f) \cdot I_O. \end{aligned} \quad (2)$$

Thus, the power conversion efficiency of the proposed driver is given by

$$\eta = \frac{P_{out}}{P_{in}} = \frac{V_f \cdot I_O}{\frac{1}{2} (V_m + V_f) \cdot I_O} = \frac{2V_f}{V_m + V_f}. \quad (3)$$

Equation (3) shows that η is nonlinearly proportional to V_f . To estimate the PF, the root mean square (RMS) value of I_{in} should be calculated first. Since I_{in} is a nonlinear function, it is divided into three sections. The time that I_{in} starts to conduct is given by

$$T_1 = \frac{T_{AC}}{2\pi} \arcsin \left(\frac{V_f}{V_m} \right). \quad (4)$$

Then, the time that I_{in} stops conducting is given by

$$T_2 = \frac{T_{AC}}{2} - T_1. \quad (5)$$

From assumption 5 and (4), C_H should be designed as

$$C_H = \frac{2I_O \cdot T_1}{V_m - V_f} = \frac{2I_O \cdot T_{AC}}{(V_m - V_f) \cdot 2\pi} \arcsin \left(\frac{V_f}{V_m} \right). \quad (6)$$

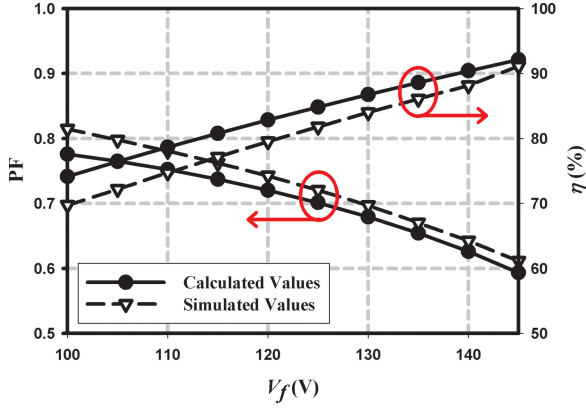


Fig. 6. Calculated and simulated variation of PF and η according to V_f for P_{in} of 10 W.

Therefore, I_{in} is given by

$$I_{in}(t) = \begin{cases} \left[\begin{aligned} &C_H \cdot \frac{dV_{in}}{dt} + I_O \\ &= \left(I_O + C_H \cdot \omega \cdot V_m \cdot \cos(2\pi t/T_{AC}) \right) \end{aligned} \right], \\ \text{for } T_1 < t \leq \frac{T_{AC}}{4} \\ I_O, \text{ for } \frac{T_{AC}}{4} < t \leq T_2 \\ 0, \text{ otherwise.} \end{cases} \quad (7)$$

The RMS value of I_{in} is then given by

$$I_{rms} = \sqrt{\frac{2}{T_{AC}} \left\{ \int_0^{T_{AC}/2} I_{in}^2(t) \cdot dt \right\}} \\ = \sqrt{\frac{2}{T_{AC}} \left\{ \int_{T_{AC}/4}^{T_2} I_O^2 \cdot dt + \int_{T_1}^{T_{AC}/4} \left(I_O + C_H \cdot \omega \cdot V_m \cdot \cos(2\pi t/T_{AC}) \right)^2 \cdot dt \right\}}. \quad (8)$$

From (2) and (8), the PF is given by

$$PF = \frac{P_{in}}{V_{rms} \cdot I_{rms}} = \frac{(V_m + V_f) \cdot I_O}{\sqrt{2} V_m \cdot I_{rms}} \\ = \frac{(V_m + V_f) \cdot I_O}{\sqrt{2} V_m \sqrt{\frac{2}{T_{AC}} \left\{ \int_{T_{AC}/4}^{T_2} I_O^2 \cdot dt + \int_{T_1}^{T_{AC}/4} \left(I_O + C_H \cdot \omega \cdot V_m \cdot \cos(2\pi t/T_{AC}) \right)^2 \cdot dt \right\}}} \quad (9)$$

Equation (9) shows that the PF is a function of V_f for a fixed P_{in} . As a design example, for an input power of 10 W with a 120-V/60-Hz ac supply, I_O is chosen to make $P_{in} = 10$ W for each given value of V_f based on (2). Fig. 6 shows a plot of the PF and η as a function of V_f based on the simulations and the equations derived above, revealing good correlation considering

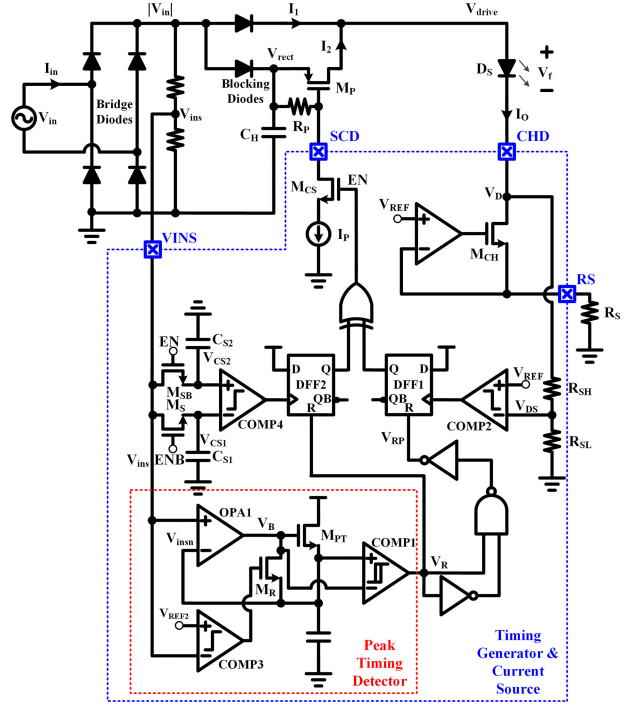


Fig. 7. Proposed LED driver with a detailed schematic diagram of the timing generator.

the assumptions and approximations in the equations. Fig. 6 indicates that a smaller V_f yields a better PF. Obviously, this is because a smaller V_f increases the period during which the input current is generated and reduces the input peak current. On the other hand, a smaller V_f degrades η due to the increase in mismatch between V_f and V_{drive} shown in Fig. 4(a). The increased voltage difference $V_{drive} - V_f = V_{loss}$ drops across I_O , shown in Fig. 4(a), and power loss increases. The decreased η affects the luminous efficacy. For example, if η changes from 80 to 70%, the luminous efficacy changes from 96 to 84 lm/W for a general mid-power white LED of 120 lm/W. Therefore, V_f should be chosen to make the PF greater than 0.7 (ENERGY STAR specifications) while maximizing η . In real implementations, the PF can be slightly higher than the simulation or calculation results since the series resistances including a thermistor in front of C_H for surge and inrush current protection help to filter out the higher order harmonics of I_{in} .

C. Operational Principles of Timing Generator

Fig. 7 shows the proposed LED driver with a circuit schematic diagram of the timing generator where the current source is implemented by a current regulation loop using an operational amplifier and a P-MOSFET M_P , which represents SW_1 in Fig. 4. The current I_O generated by the current regulation loop depends on the values of the reference voltage V_{REF} and the external resistor R_S ($I_O = V_{REF}/R_S$). The purpose of the timing generator is to control the ON/OFF timing of M_P by determining whether V_{in} is large enough to drive D_S . The ON/OFF timing is used to determine whether the LED current is supplied from V_{in} or C_H . The minimum required value of V_{in} to drive D_S is

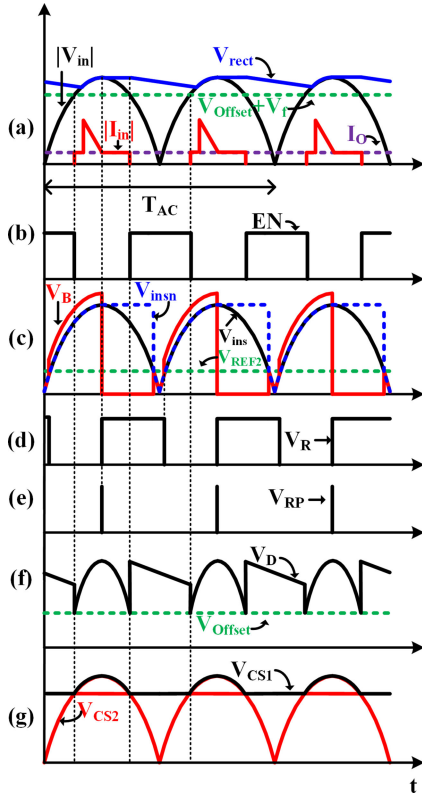


Fig. 8. Key waveforms of the timing generator.

given by

$$V_{in} > V_{REF} + V_{DS,SAT} + V_f = V_{Offset} + V_f \quad (10)$$

where $V_{DS,SAT}$ is the saturation voltage of the channel transistor M_{CH} , and V_{Offset} the sum of V_{REF} and $V_{DS,SAT}$ which is set to 10 V for the given design example. The simplest way to control the ON/OFF timing of M_P is to simply compare V_{in} with a fixed reference voltage such as $V_{Offset} + V_f$. However, when the ON/OFF timing of M_P is controlled by monitoring V_{in} only, the PF cannot be maximized since the variation of V_f is not accurately reflected on the fixed reference voltage. Thus, in the proposed LED driver in Fig. 7, the ON/OFF timing of M_P is determined by monitoring V_{in} and drain voltage V_D of M_{CH} to reflect the variation of V_f indirectly. In other words, when V_D is above V_{Offset} , where M_{CH} operates in the saturation region, the LED current is supplied from V_{in} by assuming V_{in} is sufficient to drive D_S . On the other hand, when V_D is less than V_{Offset} , where M_{CH} operates in the triode region, the LED current is supplied from C_H since V_{in} is insufficient to drive D_S . Fig. 8 shows the key waveforms of the proposed LED driver which are described in the following.

1) *Initializing Phase:* In Fig. 7, when V_{in} reaches its peak value V_m , the entire circuits are initialized. The peak point of V_{in} is detected by the peak timing detector. V_{in} is scaled down to V_{ins} to be properly processed considering the break down voltage of the given CMOS process. As shown in Fig. 8(c), until V_{ins} reaches its peak, the negative input voltage V_{insn} of the operational amplifier OPA1 tracks the positive input voltage

V_{ins} of OPA1 by a feedback loop, where the output voltage V_B of OPA1 is greater than the sum of V_{insn} and the threshold voltage of M_{PT} ($V_{th,MPT}$). Accordingly, the output V_R of the comparator COMP1 is low. At the moment that V_{ins} passes its peak, V_B starts to decrease sharply to a value lower than V_{insn} to turn OFF M_{PT} . Thus, V_R becomes high, resetting the D flip-flop DFF2, which notifies that V_{ins} is at its peak, as shown in Fig. 8(d). A short pulse is then generated at the reset pin V_{RP} of the D flip-flop DFF1 and reset DFF1, as shown in Fig. 8(e). Thereby, the signal EN becomes low, as shown in Fig. 8(b), turning OFF the switch M_{CS} and the switch M_{SB} , while the switch M_S is turned ON. V_{insn} keeps the peak value of V_{ins} since the V_{insn} node has no discharging path. Meanwhile, C_H is charged to the peak value of V_{in} .

2) *Drain Voltage Monitoring Phase:* The drain voltage monitoring phase determines the transition point of M_p from OFF to ON. In Fig. 7, after V_{ins} has passed its peak, M_{CS} turns OFF and the current flowing through R_P becomes zero. Thus, M_P turns OFF since the gate-source voltage becomes zero. At this time point, the LED current is supplied from V_{in} directly since it is sufficiently large to drive D_S . Because M_S is ON, the voltage V_{CS1} across the capacitor C_{S1} tracks V_{ins} as shown in Fig. 8(g). As V_{in} gradually decreases in time, V_D also decreases. The scale down voltage V_{DS} of V_D determined by the resistive division of R_{SL} and R_{SH} , is compared with V_{REF} by the comparator COMP2. The values of R_{SL} and R_{SH} are designed as follows: $V_{Offset} \cdot (\frac{R_{SL}}{R_{SL} + R_{SH}}) = V_{REF}$. Here, since the values R_{SL} and R_{SH} are chosen to be sufficiently large, the currents flowing through them are negligible compared to the LED current. At the point where V_D is less than V_{Offset} , as shown in Fig. 8(f), the output of COMP2 changes from low to high. The output of DFF1 then becomes high and EN also subsequently becomes high. Accordingly, since M_S turns OFF, C_{S1} samples and holds V_{ins} at this moment, and V_{in} becomes equal to the sum of V_{Offset} and V_f . Meanwhile, since V_R is high, the output of DFF2 is still low regardless of the clock signal.

3) *Input Voltage Monitoring Phase:* The input voltage monitoring phase determines the transition point of M_p from ON to OFF. In Fig. 7, after V_{in} becomes lower than the sum of V_{Offset} and V_f , M_{CS} turns ON and the current flowing through R_P is equal to I_P . The voltage drop across R_P , which is set to be greater than the threshold voltage of M_P , turns ON M_P . From this time, C_H provides the current for D_S . Thereby, V_D can remain above V_{Offset} to secure the saturation region operation of M_{CH} continuously. Because M_{SB} is ON, the voltage V_{CS2} across the capacitor C_{S2} tracks V_{ins} , as shown in Fig. 8(g). As V_{ins} gradually decreases in time, at the point where V_{ins} becomes less than the reference voltage V_{REF2} , which is set to 0.1 V, the output of comparator COMP3 becomes high. Thereby, M_R turns ON to discharge V_{insn} and can track V_{ins} again. V_{ins} then continues to decrease down to zero and then increases to be greater than V_{REF2} , as shown in Fig. 8(c). At this moment, the output of COMP3 becomes low, turning OFF M_R . Thus, V_B increases and becomes greater than V_{insn} to turn ON M_{PT} , and then V_R becomes low. As V_{ins} gradually increases in time, when V_{CS2} is greater than V_{CS1} , the output of comparator COMP4

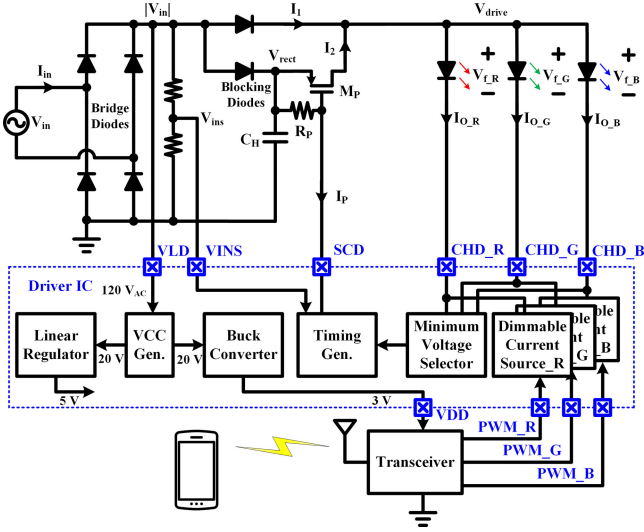


Fig. 9. Schematic of a smart bulb system adopting the proposed LED driver.

switches to high. Thereby, the output of DFF2 switches to high and then EN becomes low. At this moment, V_{in} becomes equal to the sum of $V_{O_{ffset}}$ and V_f again.

4) *Capacitor Recharging Phase*: In Fig. 7, after V_{in} becomes greater than the sum of $V_{O_{ffset}}$ and V_f , M_{CS} turns OFF causing the current flowing through R_3 to become zero. Thus, M_P turns OFF since the gate-to-source voltage is zero. Until $V_{in,s}$ reaches its peak, the LED current is directly supplied from V_{in} since V_{in} is sufficiently large to drive D_S . In addition, V_{in} gradually increases in time, such that when V_{in} becomes greater than the voltage across C_H , C_H is charged by V_{in} . Finally, when V_{in} reaches its peak, the initializing phase begins again.

III. IMPLEMENTATION DETAILS

Fig. 9 shows the schematic of a basic smart bulb system that can control the intensity of red, green, and blue (RGB) light LEDs by wireless communication and achieves flicker-free performance, an improved PF, and a compact-size module by adopting the proposed LED driver. In addition, in order to enhance the expandability in smart bulb applications, the proposed system integrates a conventional buck converter of 3-V output to supply the peripheral module consisting of an RFIC, a sensor IC, an embedded processor, etc., and the proposed LED driver. The proposed system operates as follows. When V_{in} is applied at the VLD pin, the regulated voltage V_{CC} of nominal 20 V is generated by the VCC generation block. The linear regulator then provides 5-V output to supply subblocks in the driver IC from V_{CC} . Furthermore, V_{CC} is supplied to the input of the buck converter which generates 3-V output for the external Bluetooth transceiver. The transceiver generates pulse width modulation (PWM) signals that have a particular duty ratio in communication with a smart phone. The PWM signals are transferred to the dimmable current source of RGB channels. Since the LED currents are proportional to the duty ratio of each PWM signal, the light intensity of the RGB LED can be controlled by adjusting the duty ratio of the PWM signals. $V_{in,s}$, the scale-downed value of V_{in} by the external resistors, and the drain voltages of the

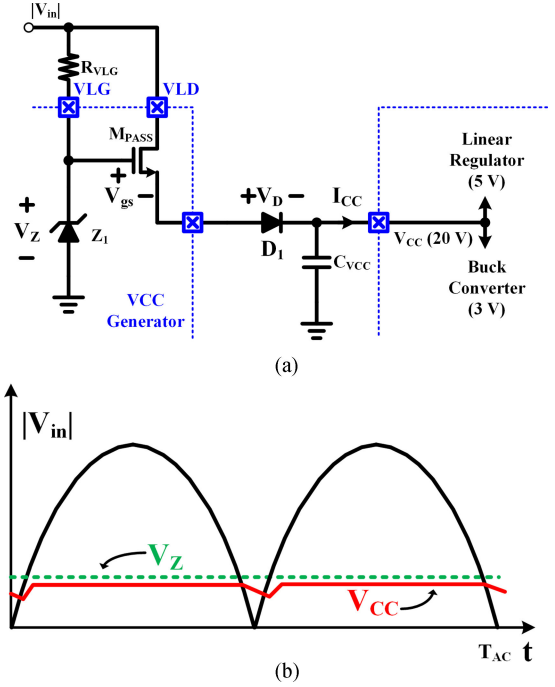


Fig. 10. VCC generator. (a) Schematic and (b) key signal waveforms.

RGB channel transistors are processed in the timing generator block to control the ON/OFF timing of the PMOS switch M_P for a maximum PF. The design details of the subblocks, shown in Fig. 9, are described in the following sections.

A. VCC Generator

Fig. 10 shows the schematic of the VCC generator and its key signal waveforms. The generator consists of a Zener diode Z_1 , a Schottky diode D_1 , a holding capacitor C_{VCC} , a pass transistor M_{PASS} , and an external resistor R_{VLG} . In Fig. 10(a), when V_{in} is greater than the output voltage of the VCC generator (V_{CC}), the required current I_{CC} for the linear regulator and the buck converter is supplied directly from V_{in} while V_{CC} keeps fixed voltage, as shown in Fig. 10(b). On the other hand, when V_{in} is less than V_{CC} , I_{CC} is supplied from C_{VCC} . The average value of V_{CC} is given by

$$\overline{V_{CC}} \cong V_Z - V_{gs} - V_D \quad (11)$$

where V_Z is the breakdown voltage of Z_1 , V_{gs} the gate-source voltage of M_{PASS} , and V_D the forward voltage drop of D_1 . R_{VLG} is used to limit the current flowing through Z_1 . In the case where the Zener diode is not available in a given technology, it can be replaced by a series of diode-connected n-MOSFETs, although the accuracy of V_{CC} will be slightly degraded.

B. Dimmable Current Source

Fig. 11 shows a schematic diagram of the dimmable current source for the red, green, and blue channels. In Fig. 11, the PWM signal comes from the external transceiver. The level shifter then changes the level of the PWM input. When the PWM signal V_{PWM} is high, the LED current I_O conducts through the channel transistor M_{CH} , whereas when V_{PWM} is low, I_O stops

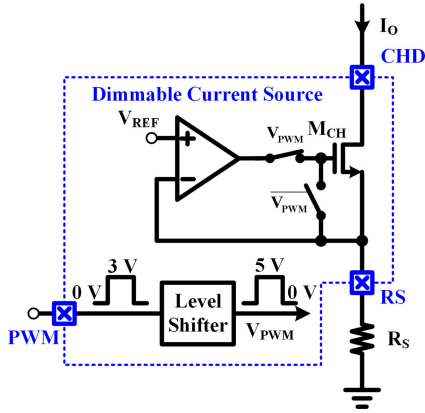


Fig. 11. Schematic diagrams of dimmable current source.

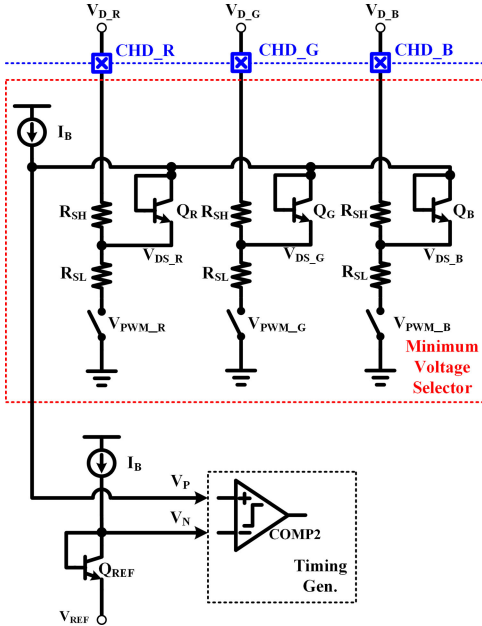


Fig. 12. Schematic diagrams of minimum voltage selector.

since the current regulation loop opens by the PWM control switches. Therefore, the average I_O can be controlled by the duty ratio of the PWM signal, which is given by

$$\overline{I_O} = D \cdot \frac{V_{REF}}{R_S} \quad (12)$$

where D is the duty ratio of the PWM signal, and R_S is the external resistor. To avoid health issues by flicker, the frequency of the PWM signal should be higher than 3 kHz [9].

C. Minimum Voltage Selector

In the proposed LED driver, the timing generator determines the ON/OFF timing of M_P by comparing the scale-downed drain voltage V_{DS} of M_{CH} with V_{REF} as shown in Fig. 7. On the other hand, since the forward voltage of the LED for each channel could vary in multichannel LED drivers, the ON/OFF timing of M_p should be determined by the LED that has the largest V_f among V_{fR} , V_{fG} , and V_{fB} . The minimum voltage selector, as shown in Fig. 12, is used to select the minimum drain

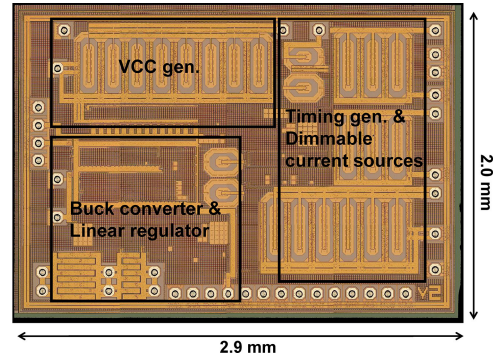


Fig. 13. Microphotograph of the proposed LED driver.

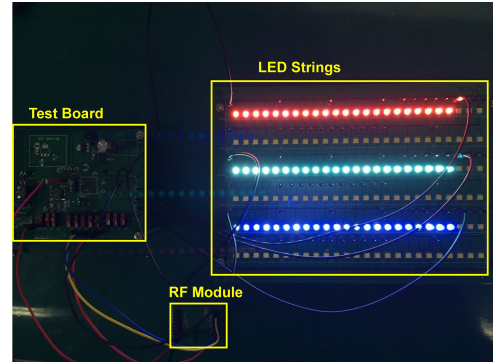


Fig. 14. Ten-Watt test board with an RF module and LED strings.

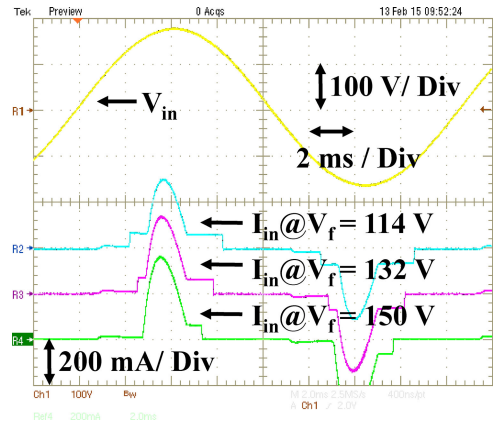


Fig. 15. Measured V_{in} and I_{in} waveforms at $V_f = 114, 132,$ and 150 V for $P_{in} = 10$ W.

voltage V_D among V_{D_R} , V_{D_G} , and V_{D_B} . In the case where V_f of one of the LEDs is the largest, V_D of that channel is smaller than that of the other two channels. The bias current I_B then flows through the NPN transistor Q of that channel only and the node voltage V_P is given by

$$V_P \cong V_D \cdot \frac{R_{SL}}{R_{SL} + R_{SH}} + V_{BE} \quad (13)$$

where V_{BE} is the base-emitter voltage of Q . In this work, I_B is set to a value smaller than one-tenth of the current flowing through R_{SH} and R_{SL} to reduce the error of V_P . The node voltage V_N is given by

$$V_N \cong V_{REF} + V_{BE,REF} \quad (14)$$

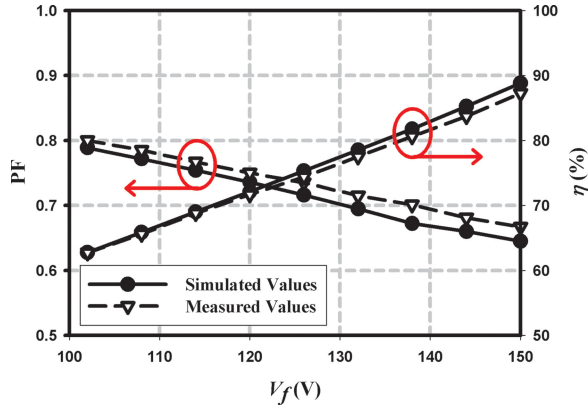


Fig. 16. Measured variation of PF and η versus V_f for $P_{in} = 10$ W in comparison with simulation.

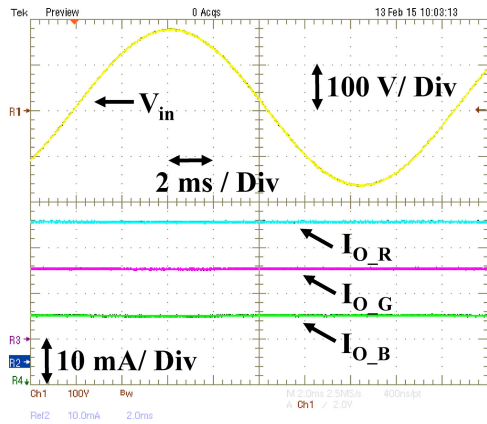


Fig. 17. Measured RGB LED current waveforms for V_f of 132 V.

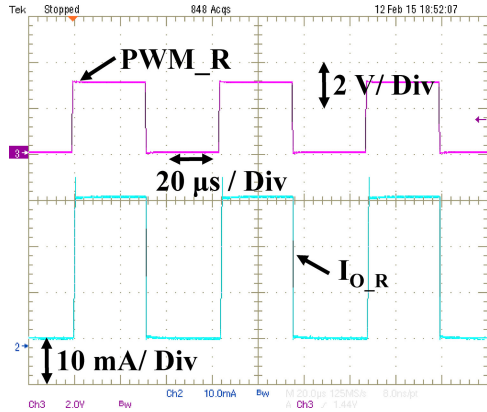


Fig. 18. Measured PWM signal and LED current waveforms of the red channel with 50% duty ratio.

where $V_{BE,REF}$ is the base-emitter voltage of Q_{REF} , which is the same as V_{BE} . The timing generator can then determine the ON/OFF timing of M_P by comparing V_P with V_N .

IV. EXPERIMENTAL RESULTS

To verify the performance of the proposed compact, flicker-free, transformer-less, multichannel, LED driver with an enhanced PF, a 10-W smart bulb prototype has been built and tested. The proposed LED driver IC is implemented in a 0.35- μ m ultrahigh voltage CMOS process. Fig. 13 shows a chip

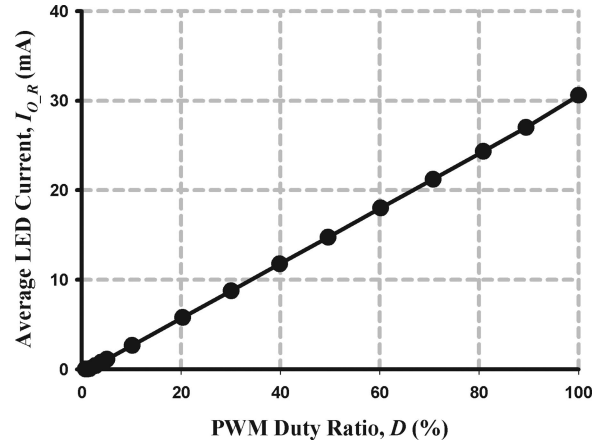


Fig. 19. Measured average LED current of the red channel over the duty ratio of the PWM signal.

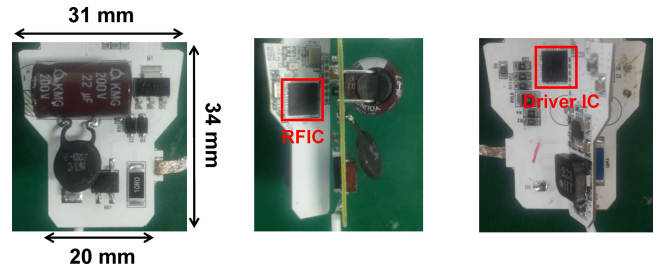


Fig. 20. Various side views of radio and driver modules of a 10-W smart bulb prototype.



Fig. 21. Group of omnidirectional smart bulb prototypes with various colors.

microphotograph of the proposed LED driver with a size of 2.9 mm \times 2.0 mm including the PADs. Fig. 14 shows the 10-W test board with a transceiver module and LED strings for V_{in} of 120 V/60 Hz. The LED strings are designed to be able to change V_f of each RGB channel where the nominal value of the forward voltage drop of each single LED is 6 V. In Fig. 14, white LEDs that are color-filtered are utilized instead of the real RGB LEDs for convenience of the measurements. Fig. 15 shows the measured V_{in} and I_{in} for $V_f = 114, 132,$ and 150 V with P_{in} being about 10 W (10.1–10.4 W), where the total RGB LED current at the maximum power is set to 60 mA ($I_{O_R} = 30$ mA,

TABLE II
PERFORMANCE COMPARISON WITH COMMERCIAL SMART BULBS

	OSRAM Lightfy RGBW LED	Philips Hue RGB LED	Cree-Connected LED	GE Link LED	LG Smart Lamp	This Work	Recommended Requirements
Watts	10	6.2	11.5	11	10	10	-
Omnidirectional performance	No	No	Yes	No	No	Yes	-
Power efficiency	N.A.	74%	84%	85%	77%	77.5%	-
Percent flicker @ $f_{AC} = 60$ Hz	N.A.	< 1%	32%	23%	< 1%	< 1%	< 4%***
PWM dimming/PWM frequency	N.A.	Yes/1 kHz	No	No	Yes/0.5 kHz	Yes/15.6 kHz	> 3 kHz [9]
Power factor	0.55*	0.49	0.99	0.94	0.54	0.715	> 0.7 [5]
Support multichannel?	Yes	Yes	No	No	No	Yes	-
Dimmable range	N.A.	N.A.	7.8–100%**	10.2–100%**	N.A.	0.7–100%	-

*From [24].

**From [25].

***No-observable-effect level: $\text{Mod\%} < 0.0333 * f_{\text{Flicker}}$ [9].

$I_{O_G} = 15$ mA, and $I_{O_B} = 15$ mA, respectively.) and the value of e-Cap is fixed at $22 \mu\text{F}$. In Fig. 15, with a decrease in V_f , the duration of nonzero I_{in} increases, while the peak value decreases. Fig. 16 shows the simulated and measured variation of PF and η versus V_f , indicating that a V_f value of 132 V could be optimal, securing a PF greater than 0.7 while maximizing η . When V_f is set to 132 V, the LED driver achieves a PF of 0.715 and η of 77.5%, respectively. As described in Section II-B, the measured PF is slightly higher than the simulated PF since the series resistances including a thermistor in front of C_H for surge and inrush current protection help to filter out the higher order harmonics of I_{in} . However, the series resistances also decrease the power conversion efficiency. In the proposed system, the driver IC consumes about 0.2 W excluding the loss at I_O and the power consumption of the transceiver is about 0.3 W, respectively, which occupy 5% of the input power (10 W). Therefore, an efficient system design is required to increase power conversion efficiency η for low power applications, especially ~ 10 W ranges. For example, a conversion ratio of the buck converter, which is used as a power supply for the transceiver shown in Fig. 9, can be increased to improve η by increasing V_{CC} . For lighting equipments with input power smaller or equal to 25 W, IEC 61000-3-2 (the international standard) requires that the third- and fifth-order harmonic currents shall not exceed 86% and 61% of the fundamental current, respectively [23]. When V_f is set to 132 V, the measured third- and fifth-order harmonic currents at the maximum power are 76% and 51%, respectively. Fig. 17 shows the measured RGB LED current waveforms at the maximum power with $V_f = 132$ V and verifies that the ripple in the LED currents is negligible. Therefore, flicker-free performance can be achieved, to the extent that even a mobile phone camera cannot find out any flicker. Fig. 18 shows the measured PWM signal (15.6 kHz) and the LED current waveform of the red channel at a duty ratio of 50%, where the duty ratio can be controlled wirelessly using a smartphone. Fig. 19 shows the measured average LED current for the red channel over the duty ratio of the PWM signal, showing a dimmable range of 0.7–100% including PWM OFF (0%). The limitation of the dimming range depends on the loop bandwidth of the dimmable current sources in Fig. 11. If a lower frequency PWM signal is

used, the lower bound of the dimming range can be expanded. Note that a PWM signal with a much lower frequency, for example, less than about 5 kHz, might cause flicker that can be visible with a camera. Fig. 20 shows the radio and driver modules of a 10-W smart bulb prototype for a V_{in} of 120 V/60 Hz, which is assembled in a 3-D manner to make better use of space. Fig. 20 verifies that the radio and driver modules can be implemented in a compact size for omnidirectional operation of indoor LED bulbs, as shown in Fig. 21. Table II compares the key performance parameters of the proposed smart bulb with those of other commercial smart bulbs which are adopting ac-dc topologies. Unfortunately, commercial smart bulbs adopting ac-direct topologies cannot be found. To the authors' best guess, it is because ac-direct types for smart bulbs have many unsolved quality issues (especially flicker) compared to ac-dc types. To compare the performances, several commercial smart bulbs are purchased and measured except the OSRAM smart bulb. In addition, some parameters are taken from the benchmark sites [24], [25]. As shown in Table II, it is difficult for the bulbs to achieve multichannel and high PF simultaneously due to bulky module size when the ac-dc LED driver is adopted. Therefore, ac-dc types without PFC, which can be considered as e-Cap types that show low PF, are often used for multichannel smart bulbs. To satisfy the no-effect level criteria, percent flicker should be less than 4% where ac line frequency is 60 Hz and PWM dimming frequency should be greater than 3 kHz [9]. As a reference, percent flicker for both incandescent lamps and compact fluorescent lamps is less than 10% [9]. Among the smart bulbs listed in Table II, only the proposed work meets this criterion. In addition, for the Philips and LG bulbs, camera flicker cannot be avoided due to the low PWM frequencies of less than 5 kHz, while the proposed work shows no camera flicker due to the high PWM frequency of 15.6 kHz. Therefore, the smart bulb reported in this work is the only one that achieves multichannel, flicker-free operation, greater than 0.7 of PF, and omnidirectional light emission simultaneously.

V. CONCLUSION

In order to achieve flicker-free performance, a high PF, and a compact module size simultaneously, a LED driver based on

a fixed LED current regulation scheme and a new PF enhancement (PFE) technique is proposed. The theoretical analysis of the proposed LED driver indicates that the LED forward voltage drop V_f has an optimal value considering the tradeoff between the PF and the power conversion efficiency as a function of V_f . The design details of a smart bulb system and its subblocks that adopt the proposed LED driver are described. To verify the proposed PFE technique, the proposed LED driver is fabricated in a 0.35- μm ultrahigh voltage CMOS process and a 10-W smart bulb prototype utilizing the chip is implemented in a compact module that allows omnidirectional performance. The measured results of the 10-W smart bulb prototype show flicker-free performance, a PF of 0.715, and power conversion efficiency of 77.5% for a 120-V ac supply. In terms of efficiency and PF only, the performance of the proposed LED driver is not state of the art where the module size has no limitation. However, the performance of the proposed LED driver can be considered as a state of the art in applications such as the omnidirectional multichannel smart bulb where the compact module size is critical.

REFERENCES

- [1] P. Middleton, P. Kjeldsen, and J. Tully, "Forecast: The internet of things, worldwide, 2013," Gartner Res., Stamford, CT, USA, 2013.
- [2] T. Komine and M. Nakagawa, "Fundamental analysis for visible-light communication system using LED lights," *IEEE Trans. Consum. Electron.*, vol. 50, no. 1, pp. 100–107, Feb. 2004.
- [3] Y. Wang, Y. Wang, N. Chi, J. Yu, and H. Shang, "Demonstration of 575-Mb/s downlink and 225-Mb/s uplink bidirectional SCM-WDM visible light communication using RGB LED and phosphor-based LED," *Opt. Exp.*, vol. 21, no. 1, pp. 1203–1208, Jan. 2013.
- [4] A. Mirvakili and V. J. Koomson, "A flicker-free CMOS LED driver control circuit for visible light communication enabling concurrent data transmission and dimming control," *Analog Integr. Circuits Signal Process.*, vol. 80, no. 2, pp. 283–292, Apr. 2014.
- [5] Environmental Protection Agency (EPA) Energy Star Program, Lamps Program Requirements Version 1.1. (2014, Aug.). [Online]. Available: <http://www.energystar.gov/products/certified-products/detail/7627/partners>
- [6] Prismark, Philips Hue Personal Wireless Lighting LED Bulbs Teardown [Online]. Available: http://www.prismark.com/whats_new.php
- [7] A. Wilkins, J. Veitch, and B. Lehman, "LED lighting flicker and potential health concerns: IEEE standard part 1789 update," in *Proc. IEEE Energy Convers. Congr. Expo.*, Sep. 12–16, 2010, pp. 171–178.
- [8] *IEEE Recommended Practices for Modulating Current in High-Brightness LEDs for Mitigating Health Risks to Viewers*, IEEE PAR1789, 2015.
- [9] B. Lehman and A. J. Wilkins, "Designing to mitigate effects of flicker in LED lighting: Reducing risks to health and safety," *IEEE Power Electron. Mag.*, vol. 1, no. 3, pp. 18–26, Sep. 2014.
- [10] M. Grotzbach, "Line side behavior of uncontrolled rectifier bridges with capacitive dc smoothing," in *Proc. Eur. Conf. Power Electron. Appl.*, 1989, pp. 761–764.
- [11] S. Wang, X. B. Ruan, K. Yao, S. C. Tan, Y. Yang, and Z. H. Ye, "A flicker-free electrolytic capacitor-less AC–DC LED driver," *IEEE Trans. Power Electron.*, vol. 27, no. 11, pp. 4540–4548, Nov. 2012.
- [12] F. Zhang, J. Ni, and Y. Yu, "High power factor AC–DC LED driver with film capacitors," *IEEE Trans. Power Electron.*, vol. 28, no. 10, pp. 4831–4840, Oct. 2013.
- [13] M. Arias, M. F. Diaz, D. G. Lamar, D. Balocco, A. A. Diallo, and J. Sebastian, "High-efficiency asymmetrical half-bridge converter without electrolytic capacitor for low-output-voltage AC–DC LED drivers," *IEEE Trans. Power Electron.*, vol. 28, no. 5, pp. 2539–2550, May 2013.
- [14] Y. Yang, X. Ruan, L. Zhang, J. He, and Z. Ye, "Feed-forward scheme for an electrolytic capacitor-less AC/DC LED driver to reduce output current ripple," *IEEE Trans. Power Electron.*, vol. 29, no. 10, pp. 5508–5517, Oct. 2014.
- [15] Y. Hu, L. Huber, and M. Jovanovic, "Single-stage, universal-input AC/DC LED driver with current-controlled variable PFC boost inductor," *IEEE Trans. Power Electron.*, vol. 27, no. 3, pp. 1579–1588, Mar. 2012.
- [16] H. H. Chou, Y. S. Hwang, and J. J. Chen, "An adaptive output current estimation circuit for a primary-side controlled LED driver," *IEEE Trans. Power Electron.*, vol. 28, no. 10, pp. 4811–4819, Oct. 2013.
- [17] S. Moon, G.-B. Koo, and G.-W. Moon, "A new control method of interleaved single-stage flyback AC–DC converter for outdoor LED lighting systems," *IEEE Trans. Power Electron.*, vol. 28, no. 8, pp. 4051–4062, Aug. 2013.
- [18] J. C. Lam and P. K. Jain, "A high power factor, electrolytic capacitor-less AC-input LED driver topology with high frequency pulsating output current," *IEEE Trans. Power Electron.*, vol. 30, no. 2, pp. 943–955, Feb. 2015.
- [19] K. Hwu and W. Tu, "Controllable and dimmable AC LED driver based on FPGA to achieve high PF and low THD," *IEEE Trans. Ind. Informat.*, vol. 9, no. 3, pp. 1330–1342, Aug. 2013.
- [20] S. Cha, D. Park, Y. Lee *et al.*, "AC/DC converter free LED driver for lightings," *IEEE Int. Conf. Consum. Electron.*, pp. 706–708, Jan. 2012.
- [21] J. Kim, J. Lee, and S. Park, "A soft self-commutating method using minimum control circuitry for multiple-string LED drivers," in *Proc. IEEE ISSCC Dig. Tech. Papers*, 2013, pp. 376–377.
- [22] N. Ning, Z. Tong, D. Yu, S. Wu, W. Chen, and C. Feng, "Highly AC voltage fluctuation-resistant LED driver with sinusoid-like reference," *J. Power Electron.*, vol. 14, no. 2, pp. 257–264, Mar. 2014.
- [23] Harmonic Current Emissions, Guidelines to the standard EN 61000-3-2. (2010, Nov.). [Online]. Available: http://www.epsma.org/pdf/PFC%20Guide_November%202010.pdf
- [24] OSRAM, OSRAM Lightify Classic A RGBW [Online]. Available: http://www.osram.com/osram_com/products/led-technology/lightify/lightify-home/lightify-lamps/lightify-classic-a-rgbw/index.jsp
- [25] Cnet, Cree Connected LED Bulb Review [Online]. Available: <http://www.cnet.com/products/cree-connected-led-bulb>



Younghun Ko received the B.S. degree in information and communications engineering, in 2010, and the M.S. degree in electrical engineering, in 2012 from the Korea Advanced Institute of Science and Technology, Daejeon, Korea, where he is currently working toward the Ph.D. degree.

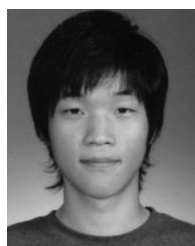
His research interests include design and analysis of power management IC, automotive IC, and LED driver IC.



Hong-Soo Cho received the B.S. degree in electrical and communications engineering from the Information and Communications University, Daejeon, Korea, in 2008, and the M.S. and Ph.D. degrees in electrical engineering from the Korea Advanced Institute of Science and Technology, Daejeon, in 2010 and 2014, respectively.

His research interests include design and analysis of CMOS RF/analog integrated circuit design. He is currently with Merlotlab Inc., Seoul, Korea, where he is a Senior Engineer responsible for the development

of LED lighting systems.



Sang-Sung Lee received the B.S. degree in information and communications engineering, and the M.S. and Ph.D. degrees in information and communications engineering from the Korea Advanced Institute of Science and Technology, Daejeon, Korea, in 2006, 2008, and 2015, respectively.

He is currently a Team manager of IC design team in Merlotlab Inc., Seoul, Korea. His main research interests include CMOS RF/analog integrated circuit (IC) design and LED driver IC design.



So-Bong Shin received the B.S. degree in electrical engineering and computer science from Handong Global University, Pohang, Korea, in 1999, and the M.S. and Ph.D. degrees in information and communications engineering from the Korea Advanced Institute of Science and Technology, Daejeon, Korea, in 2001 and 2009, respectively.

From 2005 to 2010, he was with Radiopulse Inc., Seoul, Korea, where he conducted development of RF blocks in ZigBee (IEEE802.15.4) transceiver. From 2010 to 2012, he was with Silicon Works Co., Ltd., Daejeon, where he conducted development of LED lighting systems. In 2012, he co-founded Merlot Laboratories Inc., Seoul, and is currently the CEO of the company. He is currently involved in developing smart lighting platform and its deployment to Internet of Things. His main research interests include CMOS RF/analog integrated circuit (IC) design and LED driver IC design.



Yongchul Song (S'98–M'04) received the B.S. (*summa cum laude*), M.S., and Ph.D. degrees in electrical engineering from the Korea Advanced Institute of Science and Technology, Daejeon, Korea, in 1997, 1999, and 2004, respectively.

From 2004 to 2007, he was with Samsung Electronics Company, Ltd., Gyeonggi-do, Korea, where he was involved in designing baseband modems for IEEE802.16e and 3GPP-LTE. From 2009 to 2012, he was with Radiopulse Inc., Seoul, Korea, where he conducted development of ZigBee (IEEE802.15.4) PHY transceiver. In 2012, he cofounded Merlot Laboratories Inc., Seoul, Korea, and is the CTO/VP Engineering of the company. He is currently involved in developing smart lighting platform and its deployment to Internet of Things (IoT). His research interests include architecture design and VLSI implementation of high-performance digital signal processing for communications and IoT.



Sang-Gug Lee (M'09) received the B.S. degree in electronic engineering from Kyungpook National University, Daegu, Korea, in 1981, and the M.S. and Ph.D. degrees in electrical engineering from the University of Florida, Gainesville, FL, USA, in 1989 and 1992, respectively.

In 1992, he joined Harris Semiconductor, Melbourne, FL, USA, where he was involved in silicon-based RF integrated circuit designs. From 1995 to 1998, he was with Handong University, Pohang, Korea, as an Assistant Professor with the School of Computer and Electrical Engineering. From 1998 to 2009, he was with the Information and Communications University, Daejeon, Korea, as a Professor. Since 2009, he has been a Professor with the Department of Electrical Engineering, Korea Advanced Institute of Science and Technology, Daejeon. His research interests include CMOS-based RF, analog, and mixed-mode integrated circuit (IC) designs for various radio transceiver applications. His recent research interests include low-power transceivers and extreme high-frequency (terahertz) circuit design based on CMOS technology. His other research interests include display and energy harvesting IC designs.